Vibronic fine structure in the nitrogen 1*s* photoelectron spectra of molecules from Franck-Condon simulations: Azines

Minrui Wei [1], Xiao Cheng,[2] Lu Zhang,[1] Jun-Rong Zhang [1], Sheng-Yu Wang [1], Guoyan Ge,[1]
Guangjun Tian,[3] and Weijie Hua [1,*]

[1]*MIIT Key Laboratory of Semiconductor Microstructure and Quantum Sensing, Department of Applied Physics, School of Science, Nanjing University of Science and Technology, 210094 Nanjing, China*

[2]*Hefei National Laboratory for Physical Science at the Microscale, University of Science and Technology of China, 230026 Hefei, China*

[3]*Key Laboratory for Microstructural Material Physics of Hebei Province, School of Science, Yanshan University, 066004 Qinhuangdao, China*

Vibronic coupling plays a pivotal role in molecular spectroscopy. We present a theoretical study on vibrationally resolved x-ray photoelectron spectra (XPS) of seven azines ($C_xH_yN_z$; pyridine, three diazines, two triazines, and one tetrazine) at the nitrogen 1*s* edge, to explore the vibronic coupling effects as influenced by consecutive replacement of the CH group with a N atom. Franck-Condon simulations were performed with the Duschinsky rotation effect included, where the electronic structure was calculated by the density functional theory. Validations on pyrimidine show good agreement with the experiment, weak functional dependence, and weak mode mixing effect. We observed an evident blue shift in binding energies with the increasing number of N atoms in this series, together with molecule-dependent vibronic fine structures. These molecules have either C_{2v} or C_s molecular symmetry at the optimized core-ionized geometries. Franck-Condon-active vibrational modes were identified to be low frequency (500–1650 cm^{-1}), totally symmetric (A_1 or A'), in-plane ring deformation modes. Core ionization on N* always leads to elongation of the N*−N bond length, accompanied by an increase of the ∠C−N*−X bond angle (X = C, N). Our study predicts accurate theoretical reference spectra for the azine family and provides useful information on the properties of the core-ionized states as influenced by the structural change of CH ↔ N replacement.

I. INTRODUCTION

Vibronic coupling is an essential issue in molecular electronic spectroscopy [1–4]. It brings in fingerprint fine structures on the subelectronvolt scale that contain rich information on the electronic transition and nuclear motion. In the x-ray regime, vibrationally resolved high-resolution x-ray spectra of molecules [5–16] and ions [11,17–20] in the gas phase have attracted the long interest of researchers ever since the 1960s [21]. Especially, x-ray photoelectron spectroscopy (XPS) serves as a "clean" example for interpreting the vibronic coupling effects and has received extensive research attention [5,6]. This is because XPS involves only one final electronic state (at each core center), which avoids the complexity of summing over multiple final states, for instance, in x-ray absorption spectroscopy (XAS) [16]. The vibronic fine structures in XPS carry information of the potential energy surfaces (PESs) of the initial (ground) and final (core-ionized) states and reflect the electronic and nuclear dynamics during the core ionization process.

Theoretical simulation plays an important role in interpreting the experimental fine structures. Such an interpretation can help identify the vibronic coupling effects and characterize properties of the transient core-ionized states. Among various recent theoretical developments [9–11,20,22–24], our strategy [22] that combines the density functional theory (DFT) with the full core hole (FCH) approximation and the Duschinsky rotation (DR) method [25] has been demonstrated to predict C 1*s* XPS spectra of a variety of small molecules (furan, benzene, pyridine, etc.) in excellent agreement with experiments. Besides, the usage of the DR method enables direct analysis of the short-lived core-ionized structures. The successful results encourage us to extend the FCH-DR approach for more applications.

XPS is widely used in the structural characterization of molecules and materials. There are experimental libraries that provide important references [26]. The well-known National Institute of Standards and Technology (NIST) XPS database [27] contains only binding energy (BE) information, as do some books or manuals [28,29]. It is known that BEs reported by different experiments may have inconsistencies owing to the highly arbitrary calibration procedure [30] and sometimes may vary even over 1 eV. In this sense, construction of a theoretical XPS library is important. A minilibrary for nitrogen-containing molecules and ions was recently constructed by us [31], where the focus was only N 1*s* binding energies. Spectral profiles carry richer information than just BEs. Although there are also other experimental databases [29,32–34] which contain spectra; they are mainly for various solid-state materials. There is less on high-resolution gasphase spectra. The definition of "high-resolution" develops
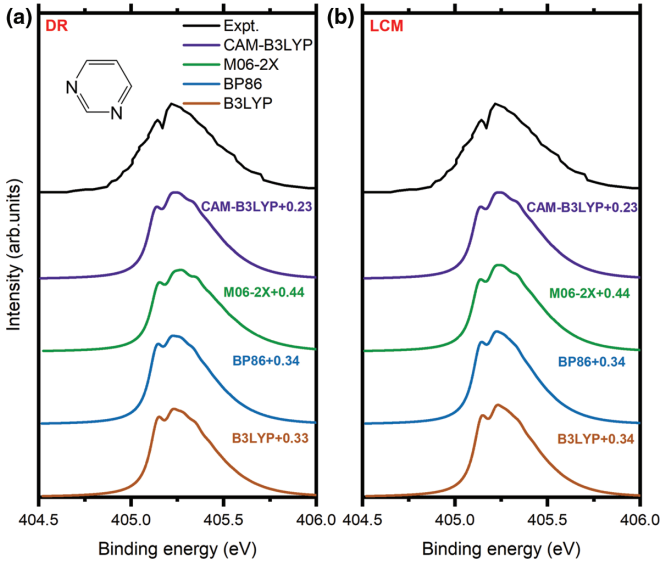

FIG. 1. Simulated N 1*s* XPS spectra of pyrimidine by using the (a) DR and (b) LCM methods with different density functionals. Spectra were convoluted with hwhm = 0.05 eV. All theoretical spectra have been added by a small *ad hoc* shift δ (labeled by numbers in eV) to better compare with the experiment [15].

with time, or rather with the development of instrumentation techniques. Gas-phase spectra usually contain sharper peaks and richer features than other phases. A theoretical library on high-precision gas-phase spectra is expected to be more helpful than just BEs in understanding the fundamental molecular physics.

The goal of this work is to extend our computational strategy to the N 1*s* edge: we report our preliminary results on a series of nitrogen-containing azine molecules, together with a detailed analysis. During the literature survey, we notice that there are fewer high-resolution XPS measurements for molecules at other edges than at the C 1*s* edge. For example, for the common molecule pyridine, to our knowledge, no high-resolution XPS spectrum at the N 1*s* edge has been reported (that at the C 1*s* edge has recently been reported [9]; and high-resolution C 1*s* XAS of pyridine has also been measured and calculated [14]). We thus wish to apply our calculations to other edges for common molecules. Azines, also known as azabenzenes, are six-membered aromatic molecules with various N substitutions on benzene (replacing one or more CH groups), with pyridine being the simplest member. They are important building blocks of proteins, nucleic acids, and energetic and optical materials. A series of azines with

varying N substitutions serve as a good model set to study the N 1*s* core ionization structures, chemical shifts, and spectral fine structures in response to systematic local structural variations. This theoretical study aims to gain general rules to understand the x-ray physics of molecules in this family.

We chose in total seven common azines for our study, including one monoazine (i.e., pyridine), three diazines (pyrimidine, pyridazine, and piperazine), two triazines (1,3,5- and 1,2,4-triazine), and one tetrazine (1,2,3,5-tetrazine). Three diazines are building blocks for designing optoelectronic materials [35–37]. Pyrimidine is the precursor of some nucleobases (uracil, thymine, and cytosine). Nitrogen-rich triazines and tetrazines are structural motifs for developing high-energy-density compounds [38–41]. 1,3,5-Triazine (i.e., *s*-triazine) is the most common triazine, which can be used in synthesizing the two-dimensional material graphitic carbon nitride (g-C_3N_4). 1,2,4,5-Tetrazine is widely used in explosives [41] and solid fuels [42].

Although there are many innershell experimental and theoretical studies on azines (pyridine [31,43–49], pyrimidine [31,47,50,51], pyrazine [31,47], pyridazine [31,47,52,53], 1,3,5-triazine [31,47,49,54], and 1,2,4,5-tetrazine [31,49]), most have been on BEs. We noticed that some BE data contain mistakes in the literature (see below) and require clarification. Regarding high-resolution experimental N 1*s* XPS spectra of azines, to our knowledge, only that on pyrimidine has been reported [50]. Here we first validate our calculations based on pyrimidine, by testing the influences of density functionals and the mode mixing effect. Then, for all molecules, we analyze the chemical shifts, fine structures, vibronic transitions, and active modes to understand the properties of the core-ionized states in this family, with respect to the local CH $\leftrightarrow$ N structural change.

II. COMPUTATIONAL METHODS

A. Franck-Condon simulations

To simulate the vibrational profiles in XPS, the harmonic oscillator approximation is assumed, and the normal vibrational modes of the ground (Q') and core-ionized (Q) electronic states, written in column vectors, are assumed to be related to each other via the Duschinsky transformation [25] as

$$Q' = \mathbf{J}Q + K. \tag{1}$$

Here we followed Sharp and Rosenstock [55] to notate the initial (ground) and final (core-ionized) electronic states with and without a prime, respectively. The Duschinsky rotation matrix

TABLE I. Vertical and adiabatic ionization potentials (I^{vert} and I^{ad}), 0-0 transition energies (E_{DR}^{00} and E_{LCM}^{00}), and difference in zero-point vibrational energies ($\Delta\varepsilon_0$) of pyrimidine simulated by the FCH method with different functionals. All energies are in electronvolts. LCM, linear coupling model; DR, Duschinsky rotation method.

Functional	I^{vert}	$I^{ad} = E_{00}^{LCM}$	E_{00}^{DR}	$\Delta\varepsilon_0$
CAM-B3LYP	405.06	404.90	404.91	0.009
M06-2X	404.88	404.69	404.71	0.015
BP86	404.96	404.79	404.80	0.012
B3LYP	404.97	404.80	404.81	0.011

TABLE II. Vertical and adiabatic ionization potentials (I^{vert} and I^{ad}), 0-0 transition energies (E_{DR}^{00} and E_{LCM}^{00}), and difference in zero-point vibrational energies ($\Delta\varepsilon_0$) of seven molecules simulated by B3LYP. Comparison was made with experiments, with relative deviations given in parentheses. All energies are in electronvolts.

Molecule		Expt.	I^{vert}	$I^{\text{ad}} = E_{00}^{\text{LCM}}$	E_{00}^{DR}	$\Delta\varepsilon_0$
Pyridine		404.70[a]/404.82[b]/404.90[c]	404.50 ($-0.20/-0.32/-0.4$)	404.26 ($-0.44/-0.56/0.64$)	404.29	0.029
Pyrimidine		405.20[c]/405.23[d]	404.97 ($-0.23/-0.26$)	404.80 ($-0.40/-0.43$)	404.81	0.011
Pyrazine		405.60[c]	405.24 (-0.36)	405.11 (-0.49)	405.12	0.012
Pyridazine		405.98[e]	405.52 (-0.46)	405.34 (-0.64)	405.35	0.011
1,3,5-Triazine		404.90[f]	405.49 ($+0.59$)	405.30 ($+0.40$)	405.30	-0.006
1,2,4-Triazine	N4	—	405.80	405.66	405.65	-0.010
	N2	—	406.01	405.83	405.82	-0.007
	N1	—	406.33	406.16	406.15	-0.008
1,2,4,5-Tetrazine		—	406.98	406.79	406.75	-0.036

[a]Pan *et al.* [46].
[b]Cavell and Allison [44].
[c]Vall-llosera *et al.* [47].
[d]Bolognesi *et al.* [50].
[e]Hannay *et al.* [53].
[f]Apen *et al.* [54].

J describes the mode mixing effect and it can be obtained from the normal coordinates (**L**′ and **L**) in the two states as $\mathbf{J} = (\mathbf{L}')^T\mathbf{L}$. The column vector $K = (\mathbf{L}')^T\mathbf{M}^{1/2}\Delta X$ describes the displacement between the two sets of potential energy surfaces, with **M** being the diagonal matrix of atomic masses and $\Delta X = X - X'$ being the change between the equilibrium geometries of the two states, respectively. The vibrational profile can be computed as long as **J**, K, and vibrational frequencies (ω' and ω) in the two electronic states are obtained. A practical approximation for vibrational profile simulations is to assume $\mathbf{J} = \mathbf{1}$ and $\omega' = \omega$, which leaves the two sets of PESs differing from each other only by a displacement (i.e., K vector) of the equilibrium positions, known as the linear coupling model (LCM) [56]. Both DR and LCM methods were simulated within a time-independent (TI) [57] framework. In comparison with various time-dependent approaches, the TI solution computes multidimensional Franck-Condon factors (FCFs) explicitly which are helpful for detailed analysis of spectral fine structures.

B. Ionic potentials

Within the LCM and DR methods, the 0-0 vibrational transition energies E_{00} are respectively given by [22],

$$E_{00}^{\text{LCM}} = I^{\text{ad}}, \tag{2}$$

$$E_{00}^{\text{DR}} = I^{\text{ad}} + \Delta\varepsilon_0, \tag{3}$$

where

$$I^{\text{ad}} = E_{\text{FCH}}|_{\textbf{min FCH}} - E_{\text{GS}}|_{\textbf{min GS}} + \delta_{\text{rel}}. \tag{4}$$

In the above equations, I^{ad} is the adiabatic IP computed according to the ΔKohn-Sham scheme [58]. **min FCH** and **min GS** denote optimized structures of the FCH (i.e., state with the removal of one electron from the core orbital) and ground states, respectively. E_{FCH} and E_{GS} are the total energies of the FCH and GS states, and $\Delta\varepsilon_0$ stands for the difference in zero-point vibrational energies of both states. δ_{rel} in Eq. (4) is a small uniform shift to consider the differential relativistic

effect related to the removal of an electron from the core orbital ($\delta_{\text{rel}} = 0.3\,\text{eV}$ was used for the N 1s core hole [58], and we call the value *after* the relativistic correction as our theoretical result). Additionally, we also computed the vertical IP (at the GS geometry) for comparison,

$$I^{\text{vert}} = E_{\text{FCH}}|_{\textbf{min GS}} - E_{\text{GS}}|_{\textbf{min GS}} + \delta_{\text{rel}}. \tag{5}$$

C. Computational details

All electronic structure calculations were performed at the DFT level with the B3LYP functional [59–61] by using the GAMESS-US software package [62,63]. Fine integration grid and tight gradient convergence tolerance (3.3×10^{-5} Hartree Bohr^{-1}) were set. A double-basis-set technique [22] was used, where for geometry relaxation and vibrational frequency calculations two different basis sets, χ_{GS} and χ_{FCH}, were used for the GS and FCH states, respectively. All energy differences [see Eqs. (4) and (5)] were calculated with the same basis set, χ_{FCH}. The cc-pVTZ basis set [64,65] was chosen for χ_{GS}. χ_{FCH} was defined based on χ_{GS}, where the triple-ζ quality individual gauge for localized orbital (IGLO-III) basis set [66] was set for the core-ionized nitrogen (N*). In systems with more than one nitrogen, the model core potential (MCP) together with the corresponding MCP/TZP basis set [67–69] was employed for each nonexcited nitrogen, which avoids the mixing of N 1s orbitals. The choice of basis sets followed a previous work [22], where assessment on basis sets based on benzene had validated its accuracy in reproducing the experimental C 1s XPS fine structures. FCH calculations were performed with restricted occupations to avoid variational collapse.

Consequent FCF simulations were performed by a modified [22] version of the DYNAVIB package [70] interfaced to GAMESS-US, which read DFT results of initial and final states (optimized structures, vibration frequencies, and normal modes). In practice, the FCFs were computed in terms of relative energies (taking the 0-0 transition energy as zero). The raw spectrum was then calibrated by adding absolute
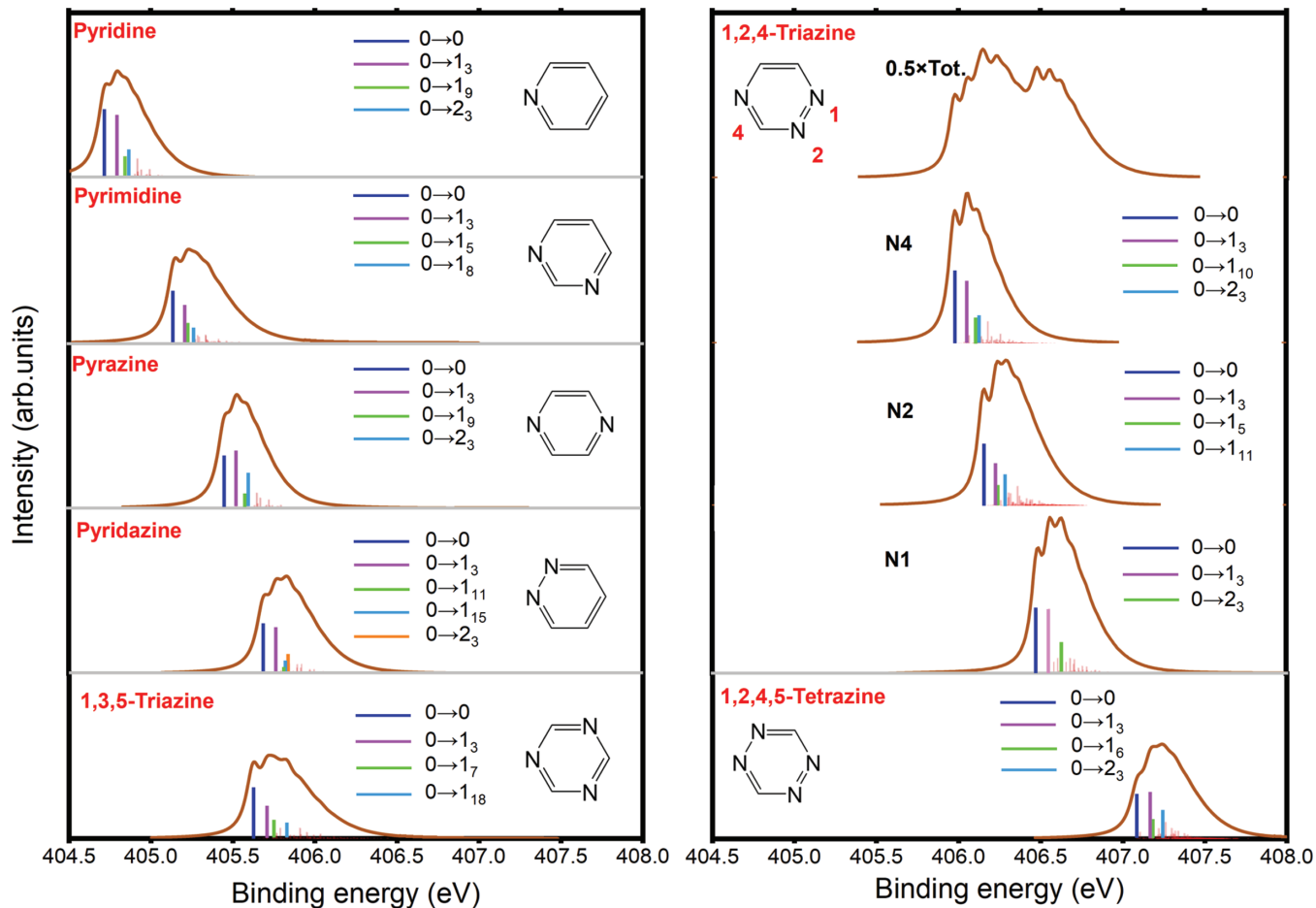
FIG. 2. Simulated vibrationally resolved N 1s XPS spectra of all azines under study by using the B3LYP-DR method. The same scale of the Y axis is used for all molecules. For 1,2,4-triazine, both atom-specific and total spectra are shown. Vertical thin lines are stick transitions. Major transitions (threshold of FCFs used: $F \geqslant 0.04$) are especially indicated with vertical thick lines in different colors (bars from left to right correspond to legends from top to bottom). For each transition, the subscript is the mode index.

0-0 transition energy, computed via Eqs. (2) and (3). Stick spectra were convoluted by a Lorentzian line shape with a half-width-at-half-maximum (hwhm) of 0.05 eV for all molecules except 1,2,4-triazine. 1,2,4-Triazine contains three nonequivalent centers (N1, N2, and N4), and a slightly smaller hwhm = 0.04 eV was used to better show the vibronic fine structures. The summation of each atom-specific spectra gives the final total spectrum.

III. RESULTS AND DISCUSSION

1. Validations on functionals for pyrimidine

Figure 1 displays vibrationally resolved XPS spectra of pyrimidine simulated by using different density functionals. Our choice of functionals covers one pure generalized gradient approximation (GGA) functional (BP86 [60,71]), two hybrid GGA functionals (B3LYP [59–61] and CAM-B3LYP [72]), and one meta GGA functional (M06-2X [73–75]). In both Duschinsky rotation [Fig. 1(a)] and linear coupling model [Fig. 1(b)] calculations, it is found that all functionals predict very similar spectral profiles with only a small deviation (at most 0.2 eV) in absolute binding energies, showing a weak influence of functionals. Besides, the similarity between DR and LCM curves also indicates a weak mode mixing effect here. The experimental spectrum [15] featured two peaks at 405.15 and 405.20 eV, with a separation of 0.05 eV. Our theoretical spectra agree well with the experiment.

Table I lists detailed energy results computed by different functionals. These functionals predicted vertical IPs at 404.9–405.1 eV and adiabatic IPs (i.e., the 0–0 transition energy by the LCM method) at 404.7–404.9 eV, respectively. The effect of functionals to either IP is within 0.2 eV. The small deviation between both IPs by each functional (ca. 0.2 eV) indicates a small deviation of PESs between the ground and core-ionized states. The 0–0 transition energies predicted by the DR method are very close to those by predicted by the LCM method, staying at 404.7–404.9 eV. This is because the zero-point energies of the initial and final states are similar ($\Delta \varepsilon_0 \sim$ 0.01–0.02 eV). The small $\Delta \varepsilon_0$ values indicate similar curvatures of the PESs of both states. Owing to the weak sensitivity of functionals for all these energetic values and spectral profiles, to keep consistency, we simply followed our previous study [22] and used B3LYP for all consequent calculations. This does not influence our conclusions.
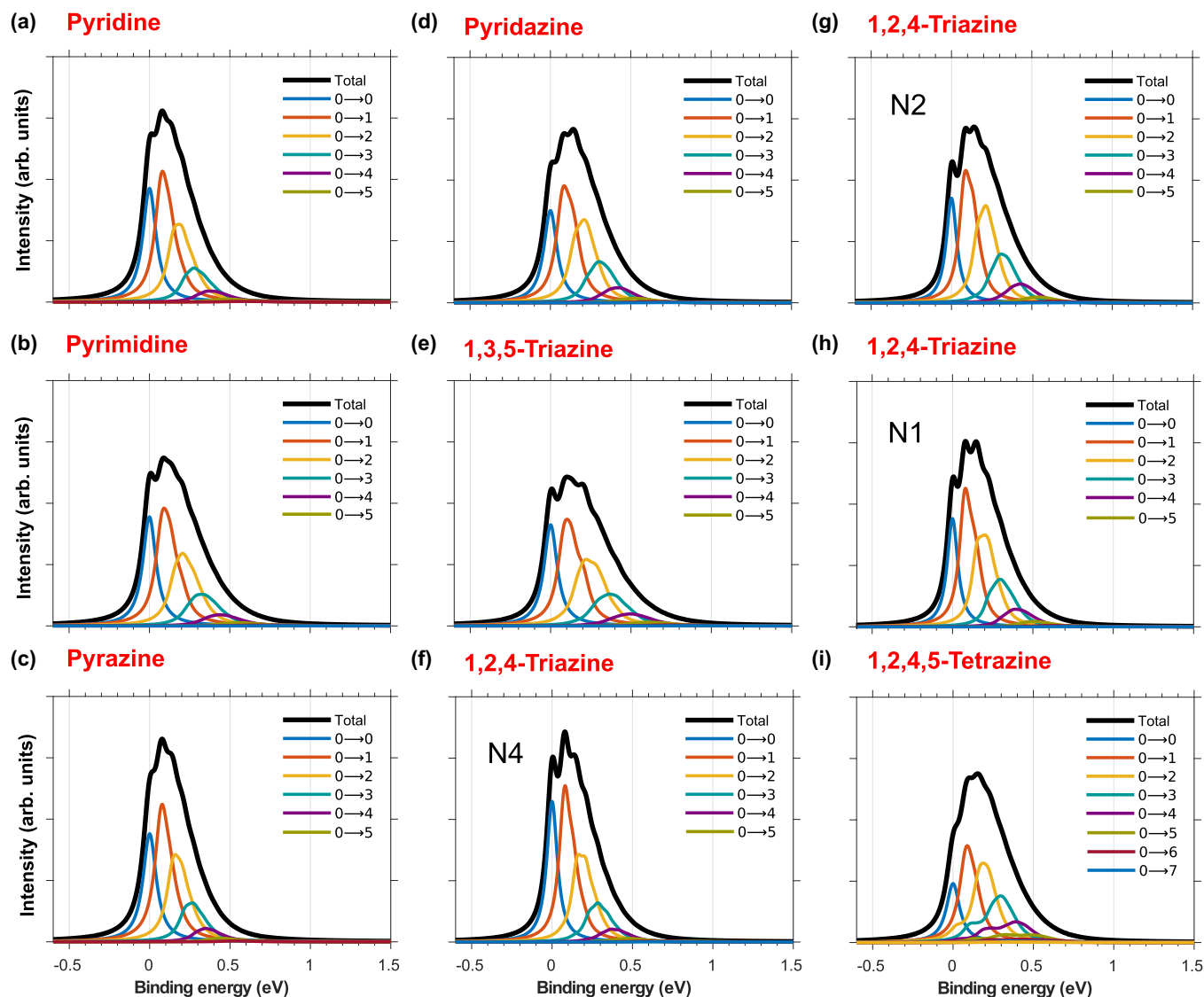
FIG. 3. Analyses of contributions of different 0-*n* transitions until convergence. 0-0 transition energy is taken as zero (i.e., relative BEs are used). Black (thick) line: Recapture of theoretical spectrum in Fig. 2. Colored (thin) lines: Individual 0-*n* transitions (from left to right, *n* = 0, 1, 2, 3, ...). The same scale of the *Y* axis is used in all panels.

2. Ionic potentials and 0-0 transition energies

Table II lists N 1*s* IPs of all the seven molecules computed by B3LYP. Generally, the vertical (adiabatic) ionic potentials cover a range of 404.5–407.0 (404.3–406.8) eV, with chemical shifts of 0.03–2.5 (0.04–2.5) eV. From mono- to tetrazine (i.e., with the increase of the number of N atoms), both IPs increase monotonically (except for a tiny violation from pyridazine to 1,3,5-triazine, where IPs of the latter drop by less than 0.1 eV). A comparison was made with available experiments: our theoretical vertical (adiabatic) IPs deviate no more than 0.6 (0.6) eV from experiments, with a mean absolute deviation (MAD) of ca. 0.4 (0.5) eV. This validates the accuracy of our simulations. Similar accuracy by DFT was predicted previously for 1*s* binding energies of light elements [31,76,77].

For isomers with close BEs, their relative values (i.e., ΔBE) were also well reproduced, with slightly better accuracy. For example, for the three diazine isomers with *meta*-, *para*-, and *ortho*-positions of the two nitrogens (i.e.,

pyrimidine, pyrazine, and pyridazine), the computed BEs (405.0, 405.2, and 405.5 eV) exhibit relative chemical shifts of 0.0, 0.3, and 0.6 eV, respectively. The results indicate the sensitivity of N 1*s* BEs subject to the CH ↔ N replacement in different positions, where the adjacent N-N group gives the largest BE. Our calculations well reproduced the BEs reported by different experiments (405.2 [15,47], 405.6 [47], and 406.0 [54] eV) with deviations of −0.2, −0.4, and −0.5 eV, respectively. It seems that the deviation of theory from experiment has the same direction for the three isomers. Hence, our predicted order is the same as the experiment, and the relative BEs agree well with the experiments (0.0, 0.4, and 0.8 eV).

It is necessary to mention that we noted a mistake for the experimental BEs of pyridazine and pyridine in the experimental work by Hannay *et al.* [53], where the same table captions were used for both molecules [78]. For this reason, the wrong number was then cited by Vall-llosera *et al.* [47] to compare with their theoretical result of pyridazine, which
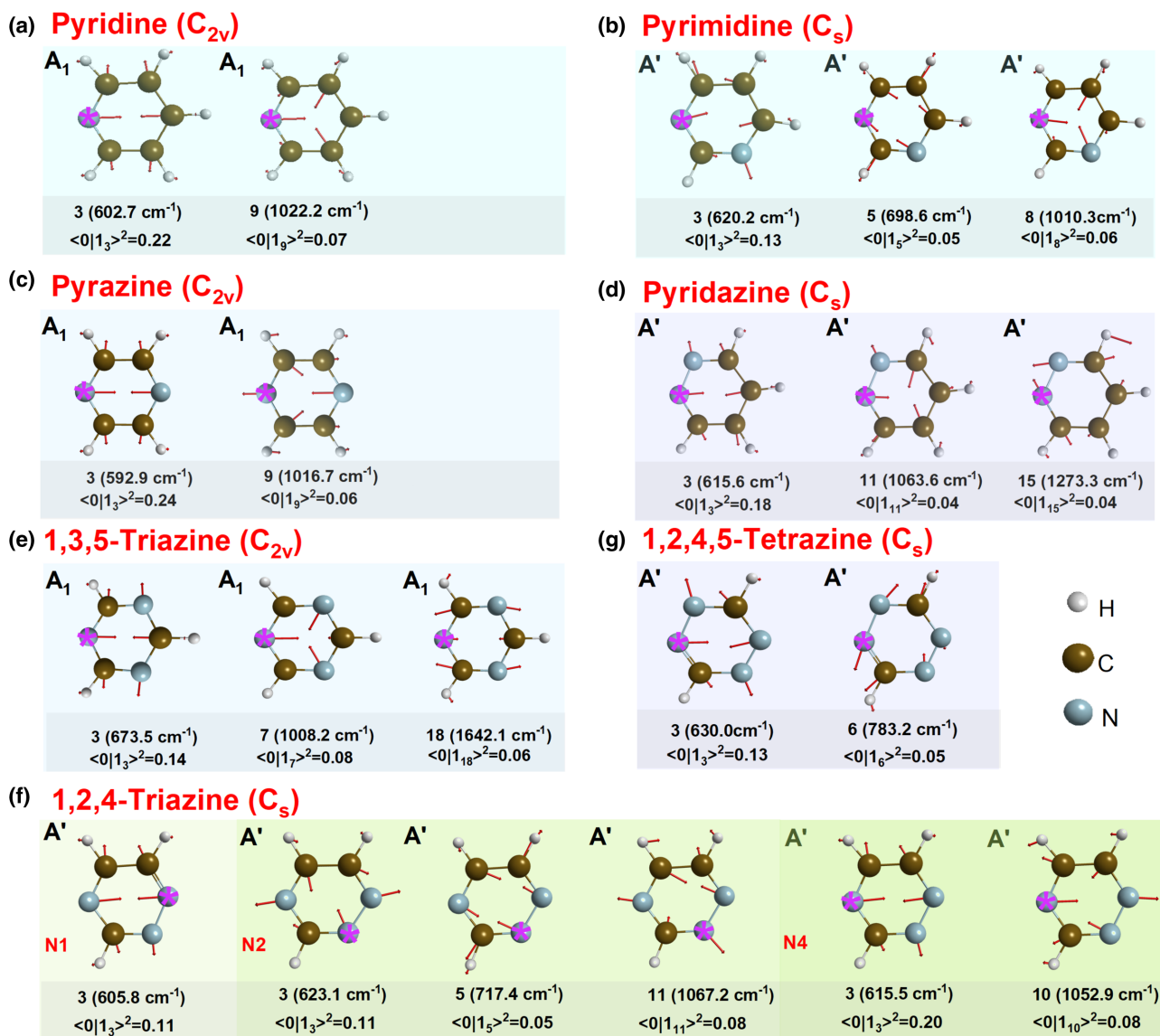
FIG. 4. Active vibrational modes for all molecules at the final state structure (**min FCH**). Molecular point group at this geometry is given in parentheses. Star denotes the ionized N center (N*). Below each figure, the mode index, the vibrational frequency (in cm^{-1}), and the corresponding FC factors (see sticks in Fig. 2) are indicated. The symmetry of each mode is indicated on the top left.

thus led to a relatively large deviation (and in the opposite direction) between experiment and theory [79]. Our calculated results (405.0, 405.2, and 405.5 eV) agree well with those by Vall-llosera *et al.* (405.0, 405.2, and 405.4 eV) and clarified this mistake in the literature.

As shown in Table II, small $\Delta\varepsilon_0$ values (-0.04–0.03 eV) were predicted. In other words, the 0-0 energies predicted by the DR and LCM methods are similar. Such results indicate weak Duschinsky rotation effects in this family. Note that in the case of the benzene C $1s$ spectrum [22], the $\Delta\varepsilon_0$ value is much larger (0.08 eV, or about twice the value), where DR and LCM spectra show larger separation in energies.

3. Vibronic fine structures and assignments

Figure 2 displays vibrationally resolved N $1s$ XPS spectra [80] of all molecules simulated by the B3LYP-DR method.

The monotonically increasing relationship between core BE and the number of N atoms is illustrated in a more vivid way. Vibrationally resolved spectra of all these molecules (atomic-specific spectra in the case of 1,2,4-triazine) show evident differences. The FC factors converge quickly at $n = 5$ in most cases ($n = 7$ for 1,2,4,5-tetrazine), subject to a convergence threshold of 0.99 used throughout the work (Fig. 3). For all these molecules, 0-1 transitions have the highest intensities, which appear at ca. 0.1 eV above each 0-0 transition. Different relative ratios of 0-0, 0-1, and 0-2 contributions tune the spectral details in each molecule, leading to several fingerprint features in the broad peak. Thus, not only the BEs but the spectral profiles are also sensitive to the CH $\leftrightarrow$ N structural variations within this family. Our calculations show that BE is the primary criterion to distinguish one structure from another in the family, but the spectral fine structures provide additional signatures for relatives with similar energies (e.g.,
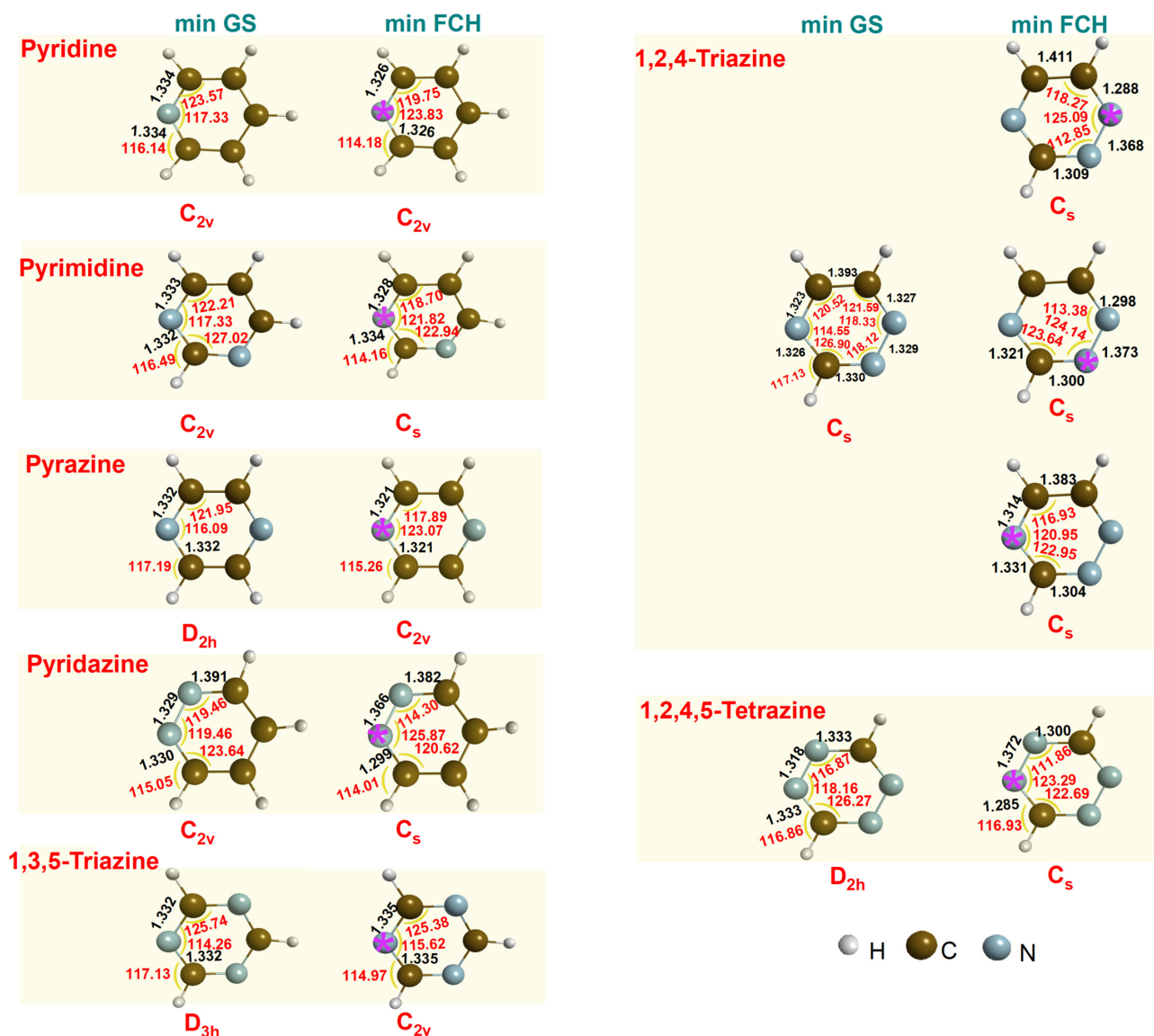
FIG. 5. Comparison of optimized geometries at the initial and final states (**min GS** and **min FCH**). At each structure, bond lengths (in Å) and angles (in degrees) near the ionized N center (N*, indicated by star) are labeled and the molecular point group is given.

pyridazine and 1,3,5-triazine). In case of relatively low experimental resolution, one will observe peak asymmetries instead of fingerprint signatures. Among these molecules, only 1,2,4-triazine contains three nonequivalent N centers, which makes its total spectrum distinctive from the total spectra of the other molecules.

Major stick transitions are also interpreted, where a threshold for FCFs, $F \geqslant 0.04$, was used to filter weak transitions. It is found that for all these molecules, only a few (1–3) vibrational modes make large contributions. For instance, for pyrimidine, three low-frequency modes, ω_3 (620 cm^{-1}), ω_5 (699 cm^{-1}), and ω_8 (1010 cm^{-1}), are Franck-Condon active. The three $0 \rightarrow 1$ transitions make major contributions to the stronger feature at 405.23 eV. The weaker feature at 405.15 eV comes from the 0-0 transition. For all these molecules, it is clear that the lowest-energy feature comes from the 0-0 transition. Those higher-energy features are mainly from 0-1 and 0-2 transitions, as illustrated in Fig. 2.

4. Active vibrational modes

Further, Fig. 4 depicts the active vibrational modes involved in Fig. 2. At the optimized core-ionized structures, these molecules belong to either the C$_{2v}$ (pyridine, pyrazine, and 1,3,5-triazine) or the C$_s$ (the rest) point group. In general, the active modes are all found to be low frequency (500–1650 cm^{-1}), in-plane ring deformation modes. They all belong to the totally symmetric irreducible representation, i.e., A_1 for C$_{2v}$ molecules or A' for C$_s$ molecules.

Similar vibrational modes can be identified in different molecules. For example, for all molecules one can always track an active ring stretching mode at ca. 590–670 cm^{-1} (ω_3 in each molecule) involving mainly N* and the atom (C or N) in its *para*-position. Besides, in most molecules (except 1,2,4,5-tetrazine or N1 ionized 1,2,4-triazine), another ring stretching mode of ca. 1000 cm^{-1} is active, involving three atoms in *meta*-positions. Interestingly, no hydrogen vibrations (either C-H stretching or bending) are found to be active.

TABLE III. Structural changes of each molecule at its optimized FCH state (**min FCH**) as compared to the optimized ground state (**min GS**). Selected bond lengths (in Å) and angles (in degrees) near the ionized nitrogen (N*) are listed (see structures and absolute structural parameters in Fig. 5).

Molecule		N*−N	N*−C (−C)[a]	N*−C (−N)[a]	∠C−N*−X[b]	∠N*−C−C	∠N*−C−N
Pyridine		—	−0.008	—	+6.50	−3.82	—
Pyrimidine		—	−0.005	+0.002	+5.85	−3.51	−4.08
Pyrazine		—	−0.011	—	+6.98	−4.06	—
Pyridazine		+0.037	−0.031	—	+6.41	−3.02	—
1,3,5-Triazine		—	—	+0.003	+1.36	—	−0.36
1,2,4-Triazine	N4	—	−0.009	+0.005	+6.40	−5.39	−3.95
	N2	+0.044	—	−0.030	+6.02	—	−3.26
	N1	+0.039	−0.039	—	+6.67	−3.32	—
1,2,4,5-Tetrazine		+0.054	—	−0.048	+5.13	—	−3.58

[a]The second nearest atom to N* is included in parentheses.
[b]$X = $ C, N.

This is consistent with the fact that in these molecules each H atom is never directly bonded to an N atom. By contrast, some C-H vibrational modes were found to be active in x-ray spectra at the C 1*s* edge, for instance, in the XPS spectrum of benzene [22], and in the XAS spectra of polycyclic aromatic hydrocarbons [16]. Such a difference in the N 1*s* and C 1*s* edges is related to the locality of core ionizations.

5. Changes in symmetry and structure

Figure 5 compares the optimized structures [80] of all molecules in the ground and core-ionized states, and Table III summarizes the essential changes near N*. Pyridine (C_{2v}) and 1,2,4-triazine (C_s) keep the same molecular symmetry in both states. While for other molecules, core ionization leads to a reduction of the molecular symmetry: $C_{2v} \rightarrow C_s$ (pyrimidine, pyridazine), $D_{2h} \rightarrow C_s$ (1,2,4,5-tetrazine), $D_{2h} \rightarrow C_{2v}$ (pyrazine), and $D_{3h} \rightarrow C_{2v}$ (1,3,5-triazine).

We also find that core ionization leads to an increase of the bond angle ∠C−N*−X ($X = $ C, N). The increment is $5.1°$–7.0 for all molecules except 1,3,5-triazine, which is only $1.4°$ (from $114.3°$ to $115.6°$). Similar increments in bond angles at the core center were found in benzene C 1*s* ionization [22]. Correspondingly, the bond angle ∠N*−C−C (∠N*−C–N) is decreased by $3.0°$–$5.4°$ ($0.4°$–$4.1°$).

Concerning the bond lengths, we found that the changes are more complex than bond angles which depend on bond types. Two types of bonds, N*−N and N*−C, are formed in these molecules. For N*−N, there is a simple general rule: these bond lengths are increased by 0.04–0.05 Å, from 1.32–1.33 Å to 1.37 Å. This is in contrast to the C 1*s* edge, where C*−X bond reductions were found in several molecules (benzene, furan, pyrrole, thiophene, pyridine) [22]. While for the N*−C bond lengths, the changes are found to be influenced by the second nearest atom (i.e., the atom one bond away): when it is carbon, i.e., N*−C (−C), the bond length is always reduced (by 0.01–0.03 Å); when it is nitrogen, i.e., N*−C (–N), both an increase and a decrease in bond lengths can be found.

IV. SUMMARY AND CONCLUSIONS

In summary, we have predicted N 1*s* vibrationally resolved spectra of seven heterocyclic azine molecules using the B3LYP-DR method and analyzed their active vibrational modes and structural changes. Tests on pyrimidine show that different density functionals generate similar spectral profiles and small deviations in binding energies, and the Duschinsky effects are weak. Within this azine family, the number and the position of N atoms strongly affect the N 1*s* BEs. A monotonically increasing relationship between core BE and the number of N atoms is found.

The underlying vibronic transitions of major peaks are analyzed in detail. It is found that the active vibrational modes of these molecules are all low-frequency (500–1650 cm^{-1}), totally symmetric in-plane modes. It is found that the introduction of the N 1*s* core hole always leads to an increase in the bond angle ∠C−N*−X and correspondingly to a decrease in ∠N*−C−X ($X = $ C, N). Concerning the bond lengths, the N*−N bonds are always stretched, while the N*−C bonds can be either stretched or shortened. Our study predicts accurate spectra of the series and provides detailed information on the properties of the core-ionized states. Simulated spectral data and Cartesian coordinates of each optimized geometry in this study are provided in the Supplemental Material [80].

[1] P. W. Atkins and R. S. Friedman, *Molecular Quantum Mechanics* (Oxford University, Oxford, 2011).

[2] J. L. McHale, *Molecular Spectroscopy* (CRC Press, Boca Raton, FL, 2017).

[3] J. Franck and E. G. Dymond, Elementary processes of photochemical reactions, Trans. Faraday Soc. **21**, 536 (1926).

[4] E. U. Condon, Nuclear motions associated with electron transitions in diatomic molecules, Phys. Rev. **32**, 858 (1928).

[5] U. Hergenhahn, Vibrational structure in inner shell photoionization of molecules, J. Phys. B: At., Mol. Opt. Phys. **37**, R89 (2004).

[6] S. Svensson, Soft x-ray photoionization of atoms and molecules, J. Phys. B: At., Mol. Opt. Phys. **38**, S821 (2005).

[7] K. Ueda, High-resolution inner-shell spectroscopies of free atoms and molecules using soft-x-ray beamlines at the third-generation synchrotron radiation sources, J. Phys. B: At., Mol. Opt. Phys. **36**, R1 (2003).

[8] U. Gelius, S. Svensson, H. Siegbahn, E. Basilier, Å. Faxälv, and K. Siegbahn, Vibrational and lifetime line broadenings in ESCA, Chem. Phys. Lett. **28**, 1 (1974).

[9] M. Mendolicchio, A. Baiardi, G. Fronzoni, M. Stener, C. Grazioli, M. de Simone, and V. Barone, Theory meets experiment for unravelling the C1s X-ray photoelectron spectra of pyridine, 2-fluoropyridine, and 2,6-difluoropyridine, J. Chem. Phys. **151**, 124105 (2019).

[10] I. Ljubić, M. T. Cvitaš, C. Grazioli, M. Coreno, S. Kazazić, and I. Novak, Vibrationally resolved valence and core photoionization and photoexcitation spectra of an electron-deficient trivalent boron compound: The case of catecholborane, Phys. Chem. Chem. Phys. **22**, 25396 (2020).

[11] R. C. Couto, W. Hua, R. Lindblad, L. Kjellsson, S. L. Sorensen, M. Kubin, C. Bülow, M. Timm, V. Zamudio-Bayer, B. von Issendorff, J. Söderström, J. T. Lau, J.-E. Rubensson, H. Ågren, and V. Carravetta, Breaking inversion symmetry by protonation: Experimental and theoretical NEXAFS study of the diazynium ion, N$_2$H$^+$, Phys. Chem. Chem. Phys. **23**, 17166 (2021).

[12] I. Minkov, F. Gel'Mukhanov, R. Friedlein, W. Osikowicz, C. Suess, G. Öhrwall, S. L. Sorensen, S. Braun, R. Murdey, W. R. Salaneck, and H. Ågren, Core excitations of naphthalene: Vibrational structure versus chemical shifts, J. Chem. Phys. **121**, 5733 (2004).

[13] K. J. Børve, L. J. Sæthre, T. D. Thomas, T. X. Carroll, N. Berrah, J. D. Bozek, and E. Kukk, Vibronic structure in the carbon 1s photoelectron spectra of HCCH and DCCD, Phys. Rev. A **63**, 012506 (2000).

[14] C. Kolczewski, R. Püttner, O. Plashkevych, H. Ågren, V. Staemmler, M. Martins, G. Snell, A. S. Schlachter, M. Sant'Anna, G. Kaindl, and L. G. M. Pettersson, Detailed study of pyridine at the C1s and N1s ionization thresholds: The influence of the vibrational fine structure, J. Chem. Phys. **115**, 6426 (2001).

[15] P. Bolognesi, P. O'Keeffe, Y. Ovcharenko, M. Coreno, L. Avaldi, V. Feyer, O. Plekan, K. C. Prince, W. Zhang, and V. Carravetta, Pyrimidine and halogenated pyrimidines near edge x-ray absorption fine structure spectra at C and N K-edges: experiment and theory, J. Chem. Phys. **133**, 034302 (2010), and Fig. 4 therein, with the experimental N1s XPS spectrum of pyrimidine in the gas phase, has been recaptured in our Fig. 1.

[16] G. Fronzoni, O. Baseggio, M. Stener, W. Hua, G. Tian, Y. Luo, B. Apicella, M. Alfé, M. de Simone, A. Kivimäki, and M. Coreno, Vibrationally resolved high-resolution NEXAFS and XPS spectra of phenanthrene and coronene, J. Chem. Phys. **141**, 044313 (2014).

[17] V. Carravetta, R. C. Couto, and H. Ågren, X-ray absorption of molecular cations—a new challenge for electronic structure theory, J. Phys.: Condens. Matter **34**, 363002 (2022).

[18] J.-P. Mosnier, E. T. Kennedy, P. van Kampen, D. Cubaynes, S. Guilbaud, N. Sisourat, A. Puglisi, S. Carniato, and J.-M. Bizau, Inner-shell photoexcitations as probes of the molecular ions CH$^+$, OH$^+$, and SiH$^+$: Measurements and theory, Phys. Rev. A **93**, 061401(R) (2016).

[19] R. Lindblad, L. Kjellsson, R. C. Couto, M. Timm, C. Bülow, V. Zamudio-Bayer, M. Lundberg, B. von Issendorff, J. T. Lau, S. L. Sorensen, V. Carravetta, H. Ågren, and J.-E. Rubensson, X-Ray Absorption Spectrum of the N$_2^+$ Molecular Ion, Phys. Rev. Lett. **124**, 203001 (2020).

[20] S. Carniato, J.-M. Bizau, D. Cubaynes, E. T. Kennedy, S. Guilbaud, E. Sokell, B. McLaughlin, and J.-P. Mosnier, Vibrationally and spin-orbit-resolved inner-shell X-ray absorption spectroscopy of the NH$^+$ olecular Ion: Measurements and ab initio calculations, Atoms **8**, 67 (2020).

[21] K. Siegbahn, *ESCA Applied to Free Molecules* (North-Holland, Amsterdam, 1969).

[22] W. Hua, G. Tian, and Y. Luo, Theoretical assessment of vibrationally resolved C1s X-ray photoelectron spectra of simple cyclic molecules, Phys. Chem. Chem. Phys. **22**, 20014 (2020).

[23] T. Moitra, D. Madsen, O. Christiansen, and S. Coriani, Vibrationally resolved coupled-cluster X-ray absorption spectra from vibrational configuration interaction anharmonic calculations, J. Chem. Phys. **153**, 234111 (2020).

[24] F. Montorsi, F. Segatta, A. Nenov, S. Mukamel, and M. Garavelli, Soft X-ray spectroscopy simulations with multi-configurational wave function theory: Spectrum completeness, sub-eV accuracy, and quantitative reproduction of line shapes, J. Chem. Theory Comput. **18**, 1003 (2022).

[25] F. Duschinsky, The importance of the electron spectrum in multi atomic molecules. Concerning the Franck-Condon principle, Acta Physicochim. URSS **7**, 551 (1937).

[26] B. V. Crist, XPS in industry—Problems with binding energies in journals and binding energy databases, J. Electron Spectrosc. Relat. Phenom. **231**, 75 (2019).

[27] NIST X-ray Photoelectron Spectroscopy Database, Version 4.1 compiled by A. V. Naumkin, A. Kraut-Vass, S. W. Gaarenstroom, and C. J. Powell, http://srdata.nist.gov/xps/, accessed on 2022-8-1.

[28] W. Jolly, K. Bomben, and C. Eyermann, Core-electron binding energies for gaseous atoms and molecules, At. Data Nucl. Data Tables **31**, 433 (1984).

[29] C. D. Wagner, *Handbook of X-Ray Photoelectron Spectroscopy: A Reference Book of Standard Data for Use in X-Ray Photoelectron Spectroscopy* (Perkin-Elmer, Eden Prairie, 1979).

[30] G. Greczynski and L. Hultman, X-ray photoelectron spectroscopy: Towards reliable binding energy referencing, Prog. Mater. Sci. **107**, 100591 (2020).

[31] X. Du, S.-Y. Wang, M. Wei, J.-R. Zhang, G. Ge, and W. Hua, A theoretical library of N1s core binding energies of polynitrogen molecules and ions in the gas phase, Phys. Chem. Chem. Phys. **24**, 8196 (2022).

[32] XPS International, https://www.xpsdata.com, accessed on 2022-8-1.

[33] The XPS Library, https://xpslibrary.com/, accessed on 2022-8-1.

[34] ESpectra: Surface Science, https://espectra.aip.org/, accessed on 2022-8-1.

[35] H. Xu, R. Chen, Q. Sun, W. Lai, Q. Su, W. Huang, and X. Liu, Recent progress in metal–organic complexes for optoelectronic applications, Chem. Soc. Rev. **43**, 3259 (2014).

[36] T.-Y. Hwang, Y. Choi, Y. Song, N. S. A. Eom, S. Kim, H.-B. Cho, N. V. Myung, and Y.-H. Choa, A noble gas sensor platform: linear dense assemblies of single-walled carbon nanotubes (LACNTs) in a multi-layered ceramic/metal electrode system (MLES), J. Mater. Chem. C **6**, 972 (2018).

[37] J. Huang and G. Yu, Structural engineering in polymer semiconductors with aromatic N-heterocycles, Chem. Mater. **33**, 1513 (2021).

[38] M. Hanumantha Rao, V. D. Ghule, and K. Muralidharan, Nitrogen-rich compounds: s-triazine and tri-s-triazine derivatives as high energy materials, J. Chem. Sci. **133**, 13 (2021).

[39] Q. Yu, J. Singh, R. J. Staples, and J. M. Shreeve, Assembling nitrogen-rich, thermally stable, and insensitive energetic materials by polycyclization, Chem. Eng. J. **431**, 133235 (2022).

[40] J. Zhang, F. Bi, J. Zhang, X. Wang, Z. Yang, G. Zhang, and B. Wang, Synthetic and thermal studies of four insensitive energetic materials based on oxidation of the melamine structure, RSC Adv. **11**, 288 (2021).

[41] D. E. Chavez, M. A. Hiskey, and D. L. Naud, Tetrazine explosives, Propellants, Explos., Pyrotech. **29**, 209 (2004).

[42] I. N. Zyuzin, I. Y. Gudkova, and D. B. Lempert, Energy abilities of certain derivatives of 1,2,4,5-tetrazine N-oxides as components of solid composite rocket propellants, Russ. J. Phys. Chem. B **15**, 611 (2021).

[43] D. T. Clark and I. W. Scanlan, *Ab initio* calculations on some aspects of structure, bonding and reactivity of pyridine, phosphabenzene and arsabenzene, J. Chem. Soc., Faraday Trans. 2 **70**, 1222 (1974).

[44] R. G. Cavell and D. A. Allison, Site of protonation in aromatic and acyclic amines and acyclic amides revealed by N1s core level electron spectroscopy, J. Am. Chem. Soc. **99**, 4203 (1977).

[45] A. A. Bakke, H.-W. Chen, and W. L. Jolly, A table of absolute core-electron binding-energies for gaseous atoms and molecules, J. Electron Spectrosc. Relat. Phenom. **20**, 333 (1980).

[46] F.-M. Pan, P. C. Stair, and T. H. Fleisch, Chemisorption of pyridine and pyrrole on iron oxide surfaces studied by XPS, Surf. Sci. **177**, 1 (1986).

[47] G. Vall-llosera, B. Gao, A. Kivimäki, M. Coreno, J. Álvarez Ruiz, M. de Simone, H. Ågren, and E. Rachlew, The C 1*s* and N 1*s* near edge x-ray absorption fine structure spectra of five azabenzenes in the gas phase, J. Chem. Phys. **128**, 044316 (2008).

[48] S. Carniato and Y. Luo, Role of differential correlation energy in core ionization of pyrrole and pyridine, J. Electron Spectrosc. Relat. Phenom. **142**, 163 (2005).

[49] D. P. Chong, Computational study of the structures and photoelectron spectra of 12 azabenzenes, Can. J. Chem. **97**, 697 (2019).

[50] P. Bolognesi, G. Mattioli, P. O'Keeffe, V. Feyer, O. Plekan, Y. Ovcharenko, K. C. Prince, M. Coreno, A. Amore Bonapasta, and L. Avaldi, Investigation of halogenated pyrimidines by x-ray photoemission spectroscopy and theoretical DFT methods, J. Phys. Chem. A **113**, 13593 (2009).

[51] F. Wang, Q. Zhu, and E. P. Ivanova, Inner-shell chemical shift of DNA/RNA bases and inheritance from their parent purine and pyrimidine, J. Synchrotron Radiat. **15**, 624 (2008).

[52] D. T. Clark, R. D. Chambers, D. Kilcast, and W. K. R. Musgrave, Experimental and theoretical studies of the molecular core binding energies of some six-membered ring nitrogen heterocycles and their perchloro- and perfluoro-derivatives, J. Chem. Soc., Faraday Trans. 2 **68**, 309 (1972).

[53] C. Hannay, D. Duflot, J.-P. Flament, and M.-J. Hubin-Franskin, The core excitation of pyridine and pyridazine: An electron spectroscopy and *ab initio* study, J. Chem. Phys. **110**, 5600 (1999).

[54] E. Apen, A. P. Hitchcock, and J. L. Gland, Experimental studies of the core excitation of imidazole, 4,5-dicyanoimidazole, and s-triazine, J. Phys. Chem. **97**, 6859 (1993).

[55] T. Sharp and H. Rosenstock, Franck-Condon factors for polyatomic molecules, J. Chem. Phys. **41**, 3453 (1964).

[56] P. Macak, Y. Luo, and H. Ågren, Simulations of vibronic profiles in two-photon absorption, Chem. Phys. Lett. **330**, 447 (2000).

[57] P. T. Ruhoff and M. A. Ratner, Algorithms for computing Franck-Condon overlap integrals, Int. J. Quantum Chem. **77**, 383 (2000).

[58] L. Triguero, O. Plashkevych, L. Pettersson, and H. Ågren, Separate state vs. transition state Kohn-Sham calculations of X-ray photoelectron binding energies and chemical shifts, J. Electron Spectrosc. Relat. Phenom. **104**, 195 (1999).

[59] A. D. Becke, Density-functional exchange-energy approximation with correct asymptotic behavior, Phys. Rev. A **38**, 3098 (1988).

[60] A. D. Becke, A new mixing of Hartree–Fock and local density-functional theories, J. Chem. Phys. **98**, 1372 (1993).

[61] C. Lee, W. Yang, and R. G. Parr, Development of the Colle-Salvetti correlation-energy formula into a functional of the electron density, Phys. Rev. B **37**, 785 (1988).

[62] M. W. Schmidt, K. K. Baldridge, J. A. Boatz, S. T. Elbert, M. S. Gordon, J. H. Jensen, S. Koseki, N. Matsunaga, K. A. Nguyen, S. Su, T. L. Windus, M. Dupuis, and J. A. Montgomery, General atomic and molecular electronic structure system, J. Comput. Chem. **14**, 1347 (1993).

[63] M. S. Gordon and M. W. Schmidt, Advances in electronic structure theory: GAMESS a decade later, in *Theory and Applications of Computational Chemistry* (Elsevier, Amsterdam, 2005), pp. 1167–1189.

[64] T. H. Dunning, Gaussian basis sets for use in correlated molecular calculations. I. The atoms boron through neon and hydrogen, J. Chem. Phys. **90**, 1007 (1989).

[65] R. A. Kendall, T. H. Dunning, and R. J. Harrison, Electron affinities of the first–row atoms revisited: Systematic basis sets and wave functions, J. Chem. Phys. **96**, 6796 (1992).

[66] W. Kutzelnigg, U. Fleischer, and M. Schindler, The IGLO-method: ab-initio calculation and interpretation of NMR chemical shifts and magnetic susceptibilities, in *Deuterium and Shift Calculation* (Springer, Berlin, 1990), pp. 165–262.

[67] Y. Sakai, E. Miyoshi, M. Klobukowski, and S. Huzinaga, Model potentials for main group elements Li through Rn, J. Chem. Phys. **106**, 8084 (1997).

[68] T. Noro, M. Sekiya, and T. Koga, Contracted polarization functions for the atoms helium through neon, Theor. Chem. Acc. **98**, 25 (1997).

[69] Segmented Gaussian Basis Set, http://sapporo.center.ims.ac.jp/sapporo/, accessed on 2022-6-4.

[70] G. Tian, S. Duan, W. Hua, and Y. Luo, DynaVib, version 1.0, Royal Institute of Technology, Sweden, 2012.

[71] J. P. Perdew, Density-functional approximation for the correlation energy of the inhomogeneous electron gas, Phys. Rev. B **33**, 8822 (1986).

[72] T. Yanai, D. P. Tew, and N. C. Handy, A new hybrid exchange-correlation functional using the Coulomb-attenuating method (CAM-B3LYP), Chem. Phys. Lett. **393**, 51 (2004).

[73] Y. Zhao and D. G. Truhlar, A new local density functional for main-group thermochemistry, transition metal bonding, thermochemical kinetics, and noncovalent interactions, J. Chem. Phys. **125**, 194101 (2006).

[74] Y. Zhao and D. G. Truhlar, Density functional for spectroscopy: No long-range self-interaction error, good performance for Rydberg and charge-transfer states, and better performance on average than B3LYP for ground states, J. Phys. Chem. A **110**, 13126 (2006).

[75] Y. Zhao and D. G. Truhlar, The M06 suite of density functionals for main group thermochemistry, thermochemical kinetics, noncovalent interactions, excited states, and transition elements: Two new functionals and systematic testing of four M06-class functionals and 12 other functionals, Theor. Chem. Acc. **120**, 215 (2008).

[76] P. S. Bagus, C. Sousa, and F. Illas, Consequences of electron correlation for XPS binding energies: Representative case for C(1s) and O(1s) XPS of CO, J. Chem. Phys. **145**, 144303 (2016).

[77] N. Pueyo Bellafont, F. Illas, and P. S. Bagus, Validation of Koopmans' theorem for density functional theory binding energies, Phys. Chem. Chem. Phys. **17**, 4015 (2015).

[78] The same table captions were used in Tables III and V of Ref. [53]. From the context, we deduce that the two tables were on pyridine and pyridazine, respectively, with the experimental IPs of 404.88 and 405.98 eV.

[79] In Table 1 of Ref. [47], the wrong experimental IP value of 404.88 eV of pyridazine (which was in fact data of pyridine) was cited from Ref. [53] to compare with their calculated IP value of 405.44 eV.

[80] See Supplemental Material at http://link.aps.org/supplemental/10.1103/PhysRevA.106.022811 for Cartesian coordinates of optimized structures and data for spectra in Fig. 2.